No. M31 $C_9H_{18}NO$, Tanane (Nitroxyde tetramethyl-2,2,6,6-piperidine oxyle)

(M = 156.25; [D:174.36])

1a Ferroelectricity of tanane was first reported by Bordeaux et al. in 1973. 73Bor

b

phase	III	II	I	73Bor
state		(F)	P	
crystal system	monoclinic	orthorhombic	tetragonal	
space group	$Cm - C_s^3$	$Fdd2 - D_{2v}^{19}$	$I\bar{4}2d - D_{2d}^{12}$ [a])	[a]) 74Bor1
Θ [K]	286.7 [b]) [D: 287.5 K] [b])			[b]) 80Laj

The temperature range where the monoclinic phase III exists strongly depends on the thermal hysteresis of the specimen. Phase II is metastable against the phase III. 74Bor1

P_s || [001].

$T_{melt} \approx$ 38 °C. 73Bor

Color: orange in phase III, red in phase I 74Bor1

Density: see Table M31-002 in subsection 8a.

2a Crystal growth: vapor deposition method. 78Laj

3a Unit cell parameters:

$a = b$ = 15.80 Å, c = 8.130 Å at 22 °C (phase I); 74Bor1

a = 22.86 Å, b = 21.48 Å, c = 8.01Å at –20 ºC (phase II); 74Bor1

a = 22.64(2) Å, b = 21.71(2) Å, c = 8.030(6) Å at 0 °C (phase II); 81Cap

a = 6.62(1) Å, b = 14.36(2) Å, c = 5.88(1) Å, β = 119.1(1)° at 18 ºC (phase III) 74Bor1

for an orange thin plate crystal obtained by sublimation at 3...10 °C.

b Z = 8, 16, 2 in phases I, II, III, respectively. 74Bor1, 72Cap, 81Cap

Crystal structure in phase II: Table M31-001; Fig. M31-001.

Form of a tanane molecule: Fig. M31-002.

4 Lattice distortion: Fig. M31-003.

5a Dielectric constant: Fig. M31-004, Fig. M31-005.

c $P_s \approx 5 \cdot 10^{-3}$ C m^{-2}. 76Bas

Hysteresis loop has not been observed because of the low mobility of the domain wall. 73Bor

6a Heat capacity: Fig. M31-006.

Transition entropy: ΔS_m = 6.3...8.8 J K^{-1} mol^{-1} for II-I transition. 73Bor

8a Sound velocities: Fig. M31-007.

Elastic stiffness: Table M31-002; Fig. M31-008.

9a Birefringence: Fig. M31-009.

b Electrooptic effect: Fig. M31-010.

r_{63}^{T} = 2.75(8) $\cdot 10^{-12}$ m V^{-1} at 170 °C. 76Bas

10b Elastic stiffness and sound velocity determined from Brillouin scattering:

see Table M31-002 and Fig. M31-007 in subsection 8a.

14b	Neutron inelastic scattering: Fig. M31-011, Fig. M31-012, Fig. M31-013; see also Table M31-002 in subsection 8a and	80Laj
16	Domain switching process: see	74Bor2

Table M31-001. $C_9H_{18}NO$ (tanane). Structure [81Cap]. T = 273 K. Fractional coordinates [$\cdot 10^{-4}$] and isotropic temperature parameter B. B is defined by Eq. (e) in Introduction.

Atom	x	y	z	B [Å^2]
N	3815(1)	–1271(1)	–1769(6)	4.2
O	3393(3)	–892(3)	–1582(12)	6.1
C(2)	3720(2)	–1783(2)	–2995(5)	4.6
C(3)	4313(4)	–2054(4)	–3474(13)	7.2
C(4)	4697(3)	–2216(3)	–1969(12)	6.5
C(5)	4831(3)	–1594(4)	–1098(14)	6.7
C(6)	4279(2)	–1277(2)	–467	4.2
C(7)	3412(5)	–1516(5)	–4506(15)	8.2
C(8)	3306(4)	–2265(4)	–2181(15)	7.2
C(9)	4424(5)	–603(4)	–25(16)	7.7
C(10)	4031(3)	–1624(4)	1039(11)	6.2
H(31)	4539(7)	–1763(9)	–4234(23)	9.0
H(32)	4205(7)	–2486(7)	–4133(19)	8.8
H(41)	4526(8)	–2526(7)	–1176(25)	8.6
H(42)	5094(8)	–2351(9)	–2418(25)	11.0
H(51)	5108(6)	–1675(6)	–32(22)	8.0
H(52)	5036(6)	–1306(7)	–1904(20)	7.7
H(71)	3658(9)	–1157(7)	–5065(17)	8.2
H(72)	2992(7)	–1345(7)	–4193(23)	9.4
H(73)	3309(9)	–1851(9)	–5429(21)	9.7
H(81)	3165(8)	–2563(10)	–3173(29)	11.9
H(82)	3530(9)	–2516(7)	–1249(24)	8.4
H(83)	2918(6)	–2028(9)	–1809(23)	9.4
H(91)	4535(8)	–381(6)	–1117(28)	7.8
H(92)	4033(10)	–388(6)	554(27)	8.5
H(93)	4777(8)	–604(6)	801(26)	9.1
H(101)	3617(6)	–1387(9)	1413(20)	10.1
H(102)	3987(6)	–2021(10)	910(23)	9.0
H(103)	4303(7)	–1533(9)	2069(20)	9.5

Table M31-002. $C_9H_{18}NO$ (tanane), $C_9D_{18}NO$. $c_{\lambda\mu}$ [80Laj]. $c_{\lambda\mu}$: elastic stiffness measured by neutron inelastic scattering and Brillouin scattering. ρ: density.

Phase I (tetragonal symmetry)

T	$T-\Theta_f$	ρ	c_{11}	c_{33}	c_{12}	c_{13}	c_{44}	c_{66}
[C°]	[K]	[kg m^{-3}]	[10^{10} N m^{-2}]					
Tanane (Brillouin scattering)								
22.3	7.2	1029	0.72(2)	0.72(2)				
13.5	0	1031	0.74(2)	0.74(2)				
Deuterated tanane (Neutron inelastic scattering)								
21.5	7.2	1131	0.76(3)	0.76(3)	0.32(4)	0.32(5)	0.22(2)	0.22(1)
14.3	0.1	1133					$0.21 \leqq 0.26$	0.22(1)

Phase II (orthorhombic symmetry)

T	$T-\Theta_f$	ρ	c_{11}	c_{22}	c_{33}	c_{12}	c_{66}
[C°]	[K]	[kg m^{-3}]	[10^{10} N m^{-2}]				
Tanane (Brillouin scattering)							
13.5	0	1031	0.74(2)	0.74(2)	0.74(2)		
4.2	–9.3	1046	0.80(2)	0.82(2)	0.79(2)	0.34(4)	0.25(4)

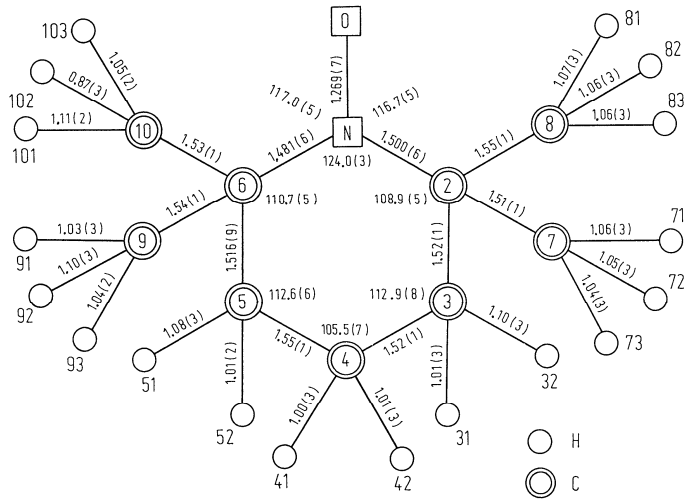

Fig. M31-001. $C_9H_{18}NO$ (tanane). Structure [81Cap]. T = 273 K. Schematic illustration of interatomic distances [Å] and bond angles [°] in a tanane molecule. See Table M31-001 for numbering of atoms.

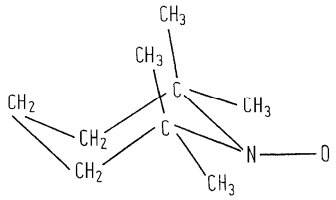

Fig. M31-002. $C_9H_{18}NO$ (tanane). Form of a molecule of tanane [73Bor].

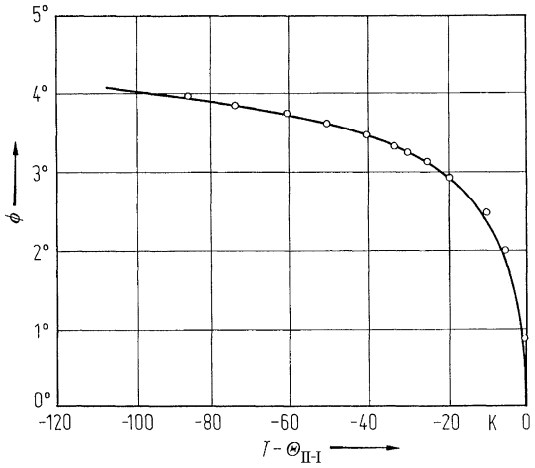

Fig. M31-003. $C_9H_{18}NO$ (tanane). ϕ vs. $T - \Theta_{II-I}$ [74Bor1]. ϕ: angle between a tetragonal axis in phase I and a pseudo-tetragonal axis in orthorhombic phase II.

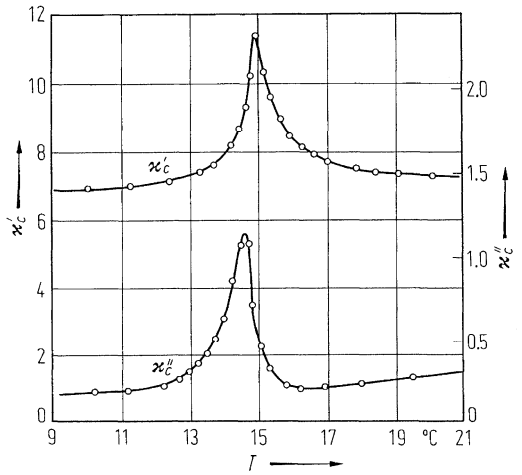

Fig. M31-004. $C_9H_{18}NO$ (tanane). κ_c', κ_c'' vs. T [74And]. f = 1.591 kHz.

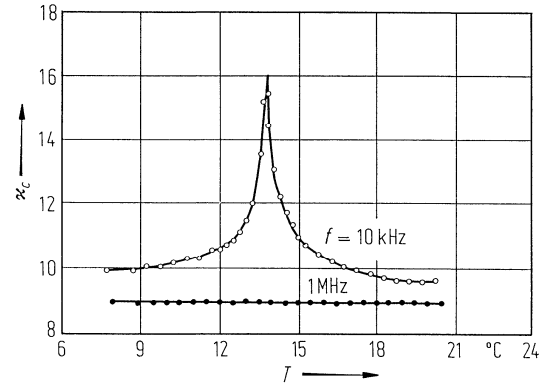

Fig. M31-005. $C_9H_{18}NO$ (tanane). κ_c vs. T at f = 10 kHz and 1 MHz [81Jan].

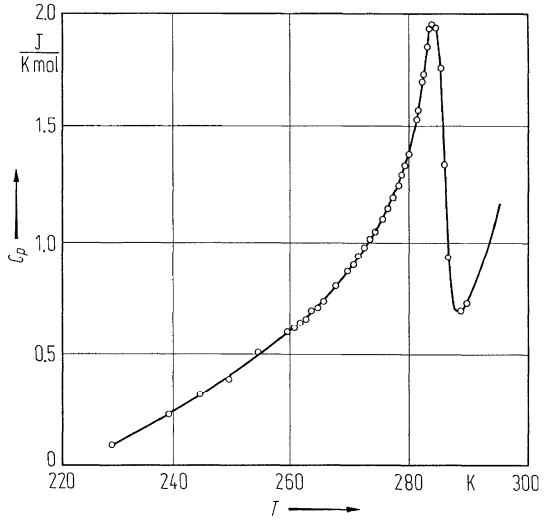

Fig. M31-006. $C_9H_{18}NO$ (tanane). C_p vs. T [73Bor].

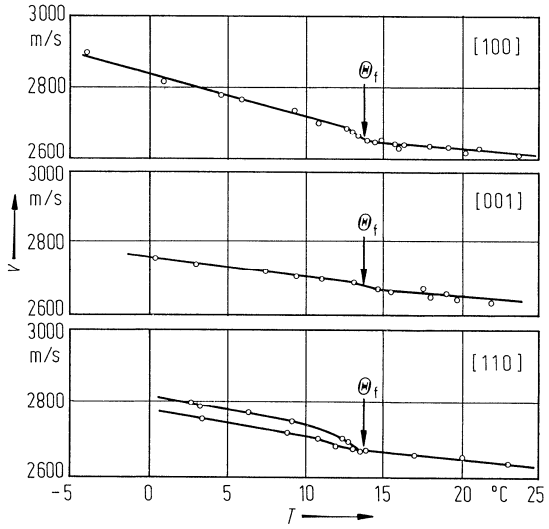

Fig. M31-007. $C_9H_{18}NO$ (tanane). v vs. T [80Laj]. v: longitudinal sound velocity deduced from Brillouin shift.

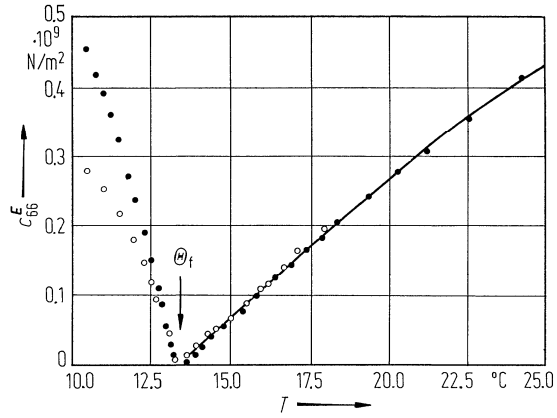

Fig. M31-008. $C_9H_{18}NO$ (tanane). c_{66}^{E} vs. T [82Leg]. c_{66}^{E}: elastic stiffness measured by resonance method. Open and full circles correspond to the measurements on different samples.

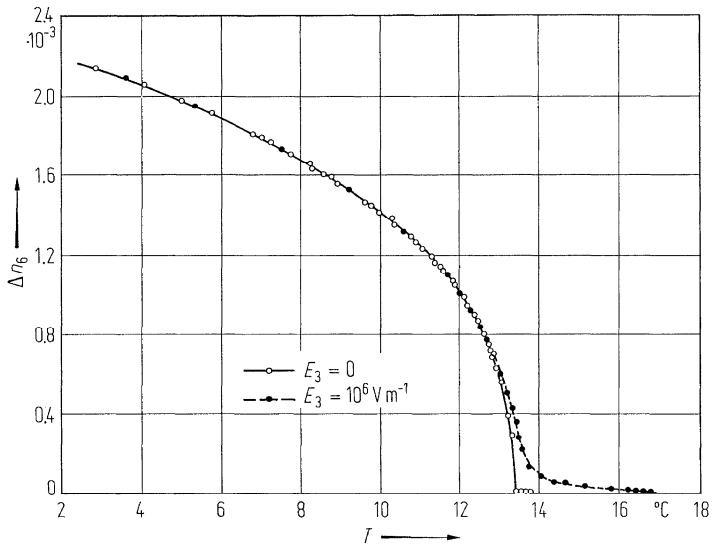

Fig. M31-009. $C_9H_{18}NO$ (tanane). Δn_6 vs. T [78Laj]. Open circles: spontaneous birefringence on a short-circuited sample. Full circles: birefringence under a dc electric field.

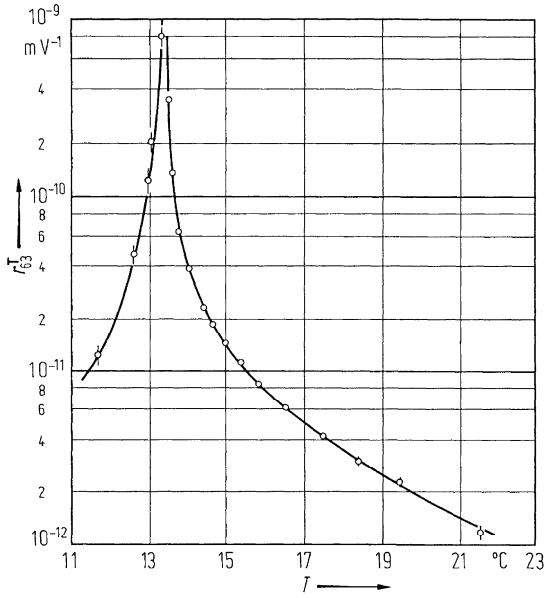

Fig. M31-010. $C_9H_{18}NO$ (tanane). r_{63}^{T} vs. T [78Laj]. r_{63}^{T} : electrooptic constants at $\lambda = 618$ nm.

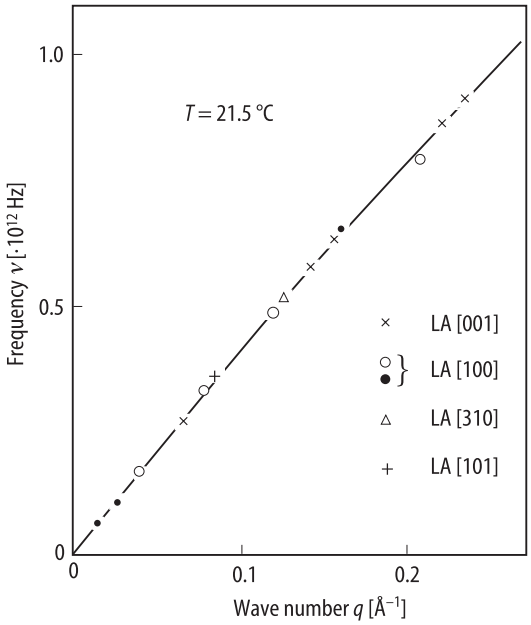

Fig. M31-011. $C_9H_{18}NO$ (tanane). ν vs. q [80Laj]. ν: frequency of longitudinal and quasi-longitudinal acoustic phonons. q: wave number of phonons obtained by constant $\boldsymbol{q}$. Cross, open circle, triangle, plus: incident neutron wave vector k_i = 2.622 Å^{-1}. Full circle: incident neutron wave vector k_i = 1.55 Å^{-1}.

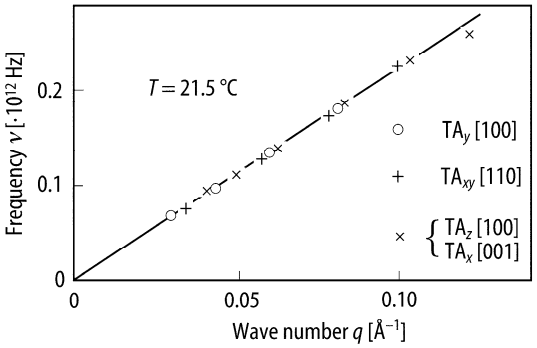

Fig. M31-012. $C_9H_{18}NO$ (tanane). ν vs. q [80Laj]. ν: frequency of transverse and quasi-transverse acoustic phonons. q: wave number of phonons obtained by constant $\boldsymbol{q}$ with incident neutron wave vector k_i = 1.55 Å^{-1}.

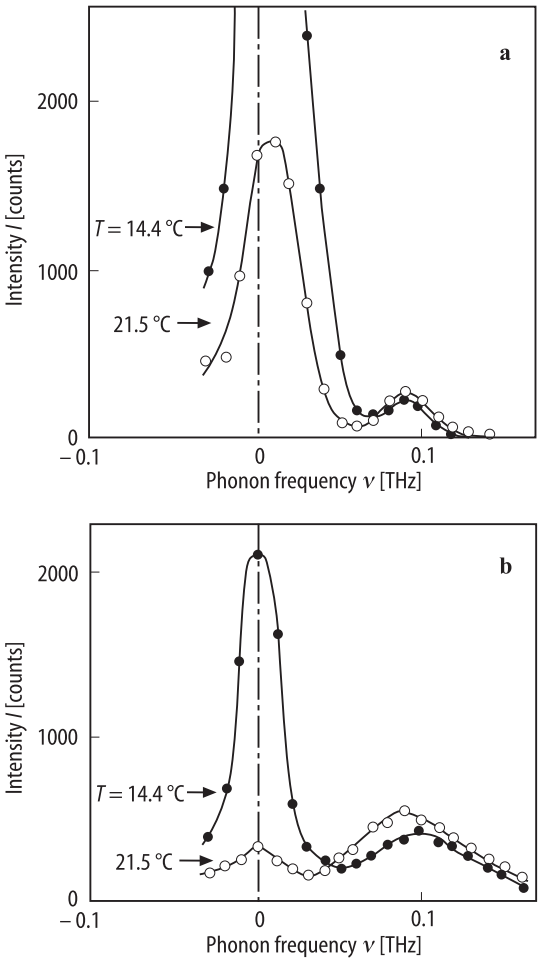

Fig. M31-013. $C_9H_{18}NO$ (tanane). I vs. ν [80Laj]. I: intensity of neutron inelastic scattering. ν: phonon frequency. Constant $\boldsymbol{q}$ scans at the points (**a**) [4, 0.1, 0] and (**b**) [0.9, 0, 3].

References

72Cap Capiomont, A., Bordeau, D., Lajzerowicz, J.: C. R. Acad. Sci. (Paris), Ser. C **275** (1972) 317.

73Bor Bordeaux, D., Bornarel, J., Capiomont, A., Lajzerowicz-Bonneteau, J., Lajzerowicz, J., Legrand, J.F.: Phys. Rev. Lett. **31** (1973) 314.

74And Anderson, A., Bastie, P., Bornarel, J., Lajzerowicz, J., Legrand, J.F.: Ferroelectrics **8** (1974) 403.

74Bor1 Bordeaux, P.D., Capiomont, A., Lajzerowicz-Bonneteau, J., Jouve, M., Thomas, M.: Acta Crystallogr. Sect. B **30** (1974) 2156.

74Bor2 Bornarel, J., Lajzerowicz, J., Legrand, J.F.: Ferroelectrics **7** (1974) 313.

76Bas Bastie, P., Bornarel, J., Lajzerowicz, J., Legrand, J.F.: Ferroelectrics **13** (1976) 319.

78Laj Lajzerowicz, J., Legrand, J.F.: Phys. Rev. B **17** (1978) 1438.

80Laj Lajzerowicz, J., Legrand, J.F., Joffrin, C.: J. Phys. (Paris) **41** (1980) 1375.

81Cap Capiomont, A., Lajzerowicz, J., Legrand, J.F., Zeyen, C.: Acta Crystallogr. Sect. B **37** (1981) 1557.

81Jan Jang, M.-S., Nakamura, T., Takashige, M., Kojima, S.: Jpn. J. Appl. Phys. **20** (1981) 661.

82Leg Legrand, J.F.: J. Phys. (Paris) **43** (1982) 1099.